ELSEVIER

International Journal of Solids and Structures 41 (2004) 1519–1538

INTERNATIONAL JOURNAL OF SOLIDS and STRUCTURES

www.elsevier.com/locate/ijsolstr

Coupled buckling and postbuckling analysis of active laminated piezoelectric composite plates

Dimitris Varelis, Dimitris A. Saravanos *

Department of Mechanical Engineering and Aeronautics, University of Patras, Patras GR 26500, Greece

Received 13 March 2003; received in revised form 12 September 2003

Abstract

A theoretical framework for analyzing the pre- and postbuckling response of composite laminates and plates with piezoactuators and sensors is presented. The mechanics include nonlinear effects due to large rotations and stress stiffening, and are incorporated into a coupled mixed-field piezoelectric laminate theory. Using the previous mechanics, a nonlinear finite element method and an incremental-iterative solution are formulated for the analysis of nonlinear adaptive plate structures subject to in-plane electromechanical loading. A novel eight-node nonlinear plate finite element is also developed. Evaluation cases predict the buckling and postbuckling response of adaptive composite beams and plates with piezoelectric actuators and sensors. The case of piezoelectric buckling and postbuckling induced by the actuators is addressed and quantified. Finally, the possibility to actively mitigate the mechanical buckling and postbuckling response of adaptive piezocomposite plates is illustrated.

Keywords: Adaptive structures; Buckling; Nonlinear; Plates; Laminated; Composite; Piezoelectric; Actuators; Sensors

1. Introduction

The need for light-weight structures in aerospace, aeronautical and automotive applications has led to the gradual replacement of many traditional isotropic materials with composites which provide both high stiffness and low weight. Additional requirements for multi-functionality, active vibration and noise control and structural health monitoring has led to the development of adaptive piezocomposite materials and structures. Buckling caused by in-plane compressive loading, combined with structural imperfections, load eccentricity or other out-of-plane loads can lead to large deflections, structural instability and finally to structural failure. Thus, the buckling of composite structures and their ability to carry loads beyond the critical point into the postbuckling range has received substantial analytical and experimental attention. For example, we mention the reviews of Leissa (1987) and Chia (1988), the models for unsymmetric plates by Jensen and Lagace (1988), the early experimental work by Starnes and Rouse (1981), the analytical work

* Corresponding author. Tel.: +30-2610996191; fax: +30-2610997234.
E-mail address: saravanos@mech.upatras.gr (D.A. Saravanos).

0020-7683/$ - see front matter © 2003 Published by Elsevier Ltd.
doi:10.1016/j.ijsolstr.2003.09.034

by Engelstad et al. (1992) on postbuckling response and failure modes of panels loaded in compression, and the recent works on dynamic instability (Tabiei and Simitses, 1997), thermomechanical buckling (Librescu et al., 2000), and the buckling of sandwich structures (Kardomateas et al., 2002; Librescu and Hause, 2000).

Buckling instability is also expected to be a critical mode of failure in adaptive structures, because of additional in-plane loads imposed by the actuators, and their anticipated multifunctional role under a variety of loading conditions. Consequently, the buckling behavior of adaptive structures requires substantial consideration, while development of new modeling and computational capabilities for analyzing the buckling and postbuckling response of smart structural components is required. While a vast number of analytical and computational models have been reported (Saravanos and Heyliger, 1999), their majority is limited to the linear region and are focused on linear static and dynamic response. Meressi and Paden (1993) performed experimental studies to design a controller for the buckling control of a beam. Thomson and Loughlan (1995) used piezoelectric actuators to actively control the buckling of composite strips. de Faria and de Almeida (1999) reported a theoretical framework and a finite element for the buckling of beams with a pair of surface attached piezoactuators using classical beam theory, and presented the enhancement of prebuckling behavior of slender beams through piezoelectric control. Varelis and Saravanos (2002a,b) reported a coupled theory and finite element for the linear buckling of piezocomposite plates under combined electromechanical loading. Pai et al. (1993) reported an uncoupled induced strain nonlinear theory for the dynamics and active control of piezoelectric plates Tzou and Bao (1997) and Tzou and Zhou (1997) reported uncoupled theoretical formulations for thermopiezoelectric plates and the active control of nonlinear deflections. Di Scuva and Icardi (1995) presented an uncoupled shear-theory based analytical solution for the large deflections of multilayered beams with piezoelectric actuators. Oh et al. (2001) presented an uncoupled layerwise finite element for the postbuckling of active thermopiezoelectric plates. Finally, Varelis and Saravanos (2002a,b) reported nonlinear mechanics and developed a finite element for the nonlinear response of active piezoelectric composite plates.

In the present paper, coupled multi-field generalized nonlinear mechanics together with an associated plate finite element are presented, for analyzing the buckling and postbuckling response of active and sensory piezoelectric-composite laminated plates, which include nonlinear effects due to large rotations and stress stiffening. In this context, coupled nonlinear governing equations for piezolaminates are initially formulated using mixed-field shear-layerwise kinematic assumptions (Saravanos, 1997). The derivation of discrete coupled nonlinear equations of motion is subsequently described using an in-plane finite element approximation, and based on this formulation a parabolic nonlinear laminated piezocomposite plate element is developed. The discrete coupled equations of motion of the smart structure are finally linearized and solved using an incremental-iterative method based on the Newton–Raphson technique. Numerical validations of the present method are shown for the cases of buckling and postbuckling of composite plates under in-plane mechanical loading. Additional numerical results illustrate the unique cases of active piezoelectric buckling of various piezocomposite beams and plates subject to unipolar electric fields on the actuators, and investigate the contribution of new nonlinear stiffness and piezoelectric terms. Finally, the buckling and postbuckling response of beams and plates under combined electromechanical loading is predicted and the possibility of active buckling compensation is investigated.

2. Laminate mechanics

2.1. Governing equations

The general case of a piezoelectric composite laminate is considered (Fig. 1a), consisting of an arbitrary configuration of linear piezoelectric layers or composite plies and undergoing large displacements and

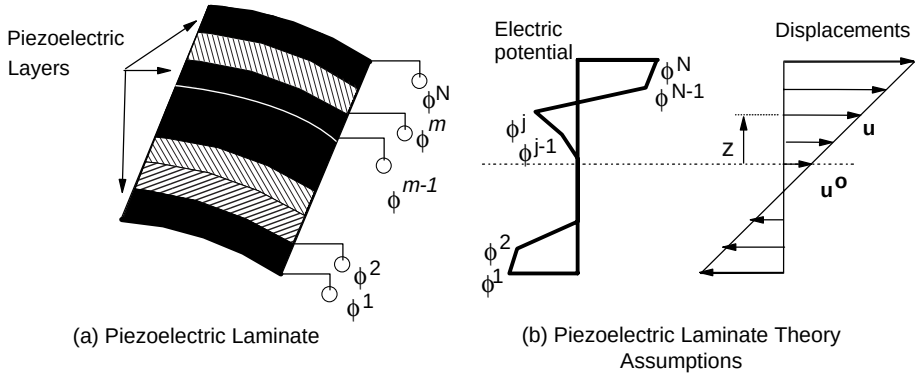

Fig. 1. Piezoelectric laminates. (a) Mixed-field kinematic assumptions; (b) assumed through the thickness displacement and electric potential fields.

rotations. Consequently, the material of each ply of the piezoelectric laminate remains within the range of linear piezoelectricity with constitutive equations of the form

$$\sigma_i = C_{ij}^E S_j - e_{ik} E_k, \qquad D_l = e_{lj} S_j + \varepsilon_{lk}^S E_k \tag{1}$$

where $i, j = 1, \ldots, 6$ and $k, l = 1, \ldots, 3$; σ_i and S_j are the mechanical stresses and engineering strains in extended vectorial notation, C_{ij} is the elastic stiffness tensor, e_{ik} is the piezoelectric tensor, E_k is the electric field vector, D_l is the electric displacement vector and ε_{lk} is the electric permittivity tensor. The previous equations describe the material behavior either on the orthogonal material axes 1, 2, 3 or the structural axes x, y and z, respectively, provided that proper transformations are applied on material property matrices. The Green–Lagrange engineering strains in each ply are assumed to have the following form

$$\begin{aligned} &S_1 = u_{,x} + \tfrac{1}{2} w_{,x}^2, \qquad S_2 = v_{,y} + \tfrac{1}{2} w_{,y}^2, \qquad S_6 = (u_{,y} + v_{,x}) + w_{,x} w_{,y}, \\ &S_4 = u_{,z} + w_{,x}, \qquad S_5 = v_{,z} + w_{,y}, \qquad S_3 = 0 \end{aligned} \tag{2}$$

where the first right hand side terms describe the linear strain components, while the last right hand side terms are the nonlinear strain components due to large out-of-plane rotations, respectively.

2.2. Kinematic assumptions

The kinematic assumptions of the coupled mixed-field laminate theory proposed by Saravanos (1997) are used, which represent all state variables through the laminate thickness by combining a shear-deformable linear displacement field with a discrete-layer electric potential field. The discrete-layer field divides the laminate into $N-1$ sublaminates by assuming a continuous electric potential field through each sublaminate, such that, a piecewise continuous field results through the whole thickness of the piezolaminate, as seen in Fig. 1b. The assumed displacements and electric potential have the following form through the thickness

$$\begin{aligned} &u(x,y,z,t) = u^0(x,y,t) + z\beta_x(x,y,t), \qquad v(x,y,z,t) = v^0(x,y,t) + z\beta_y(x,y,t), \\ &w(x,y,z,t) = w^0(x,y,t), \qquad \varphi(x,y,z,t) = \sum_{m=1}^{N} \varphi^m(x,y,t) \Psi^m(z) \end{aligned} \tag{3}$$

where u^0, v^0, w^0 are mid-surface displacements, β_x and β_y are rotation angles, φ^m are electric potential values describing the layerwise electric potential field, and Ψ^m are linear interpolation functions. The kinematic assumptions (3) were chosen to form the basis of the developed mechanics, because they readily enable consideration of piezoelectric laminates with arbitrary configurations of composite plies, active and sensory layers, while capturing both mechanical and electric field variables. In the context of the previous kinematic assumptions (Eq. (3)) and nonlinear strain relations (Eq. (2)), the strains through the thickness of the laminate take the following form

$$S_i = S_i^0 + zk_i^0 + S_{\mathrm{L}i}, \quad S_{\mathrm{S}j} = S_{\mathrm{S}j}^0, \qquad i = 1,2,6 \;\; j = 4,5 \tag{4}$$

where S_i^0, $S_{\mathrm{S}j}^0$ are mid-plane in-plane and shear strains respectively, and k_i^0 mid-surface curvatures (Saravanos, 1997); $S_{\mathrm{L}i}$ are the nonlinear laminate strains on the mid-surface. More details about the nonlinear strain and electric field vectors are provided in Appendix A.

2.3. Generalized equations of motion

The mechanical and electrical equilibrium of the laminated plate is represented by the stress equilibrium and the conservation of electric charge equations, respectively. Through the use of the divergence theorem, the latter can be expressed by the equivalent variational forms shown in the right hand side of the following equations

$$\begin{aligned}
&\delta\boldsymbol{u}^{\mathrm{T}}\boldsymbol{\Psi}_u = -\int_V \delta\boldsymbol{S}_i\boldsymbol{\sigma}_i\,\mathrm{d}V + \int_V \delta\boldsymbol{u}_j\boldsymbol{b}_j\,\mathrm{d}V + \int_{\Gamma_\tau} \delta\bar{\boldsymbol{u}}_j\bar{\boldsymbol{\tau}}_j\,\mathrm{d}\Gamma = 0,\\
&\delta\boldsymbol{\varphi}^{\mathrm{T}}\boldsymbol{\Psi}_e = -\int_V \delta\boldsymbol{E}_j\boldsymbol{D}_j\,\mathrm{d}V + \int_{\Gamma_q} \delta\bar{\varphi}\bar{q}\,\mathrm{d}\Gamma = 0,\\
&\quad i = 1,\ldots,6, \;\; j = 1,\ldots,3
\end{aligned} \tag{5}$$

with bold symbols indicating vectors. The vectors $\boldsymbol{\Psi}_u$, $\boldsymbol{\Psi}_e$ represent differences between internal and external forces and charges, respectively, which diminish at mechanical and electric equilibrium; $\bar{\boldsymbol{\tau}}$ are the surface tractions on the bounding surface Γ_τ, $\bar{q}$ is the electrical charge applied on the terminal bounding surface Γ_q; overbar indicates surface quantities; V represents the whole laminate volume including both composite and piezoelectric layers. Combining Eq. (5) with Eq. (4), integrating through the thickness of the piezocomposite laminate, and collecting the common generalized strain and electric field terms, the following equivalent variational forms are finally derived at the laminate level

$$\begin{aligned}
\delta\boldsymbol{u}^{\mathrm{T}}\boldsymbol{\Psi}_u = -\int_{A_0} \Big(&\delta\boldsymbol{S}^{0^{\mathrm{T}}}[A]\boldsymbol{S}^0 + \delta\boldsymbol{S}^{0^{\mathrm{T}}}[B]\boldsymbol{k}^0 + \delta\boldsymbol{k}^{0^{\mathrm{T}}}[B]\boldsymbol{S}^0 + \delta\boldsymbol{k}^{0^{\mathrm{T}}}[D]\boldsymbol{k}^0 + \delta\boldsymbol{S}_{\mathrm{S}}^{0^{\mathrm{T}}}[A_{\mathrm{S}}]\boldsymbol{S}_{\mathrm{S}}^0\\
&+ \delta\boldsymbol{S}^{L^{\mathrm{T}}}[A]\boldsymbol{S}^0 + \delta\boldsymbol{S}^{L^{\mathrm{T}}}[A]\boldsymbol{S}^L + \delta\boldsymbol{S}^{L^{\mathrm{T}}}[B]\boldsymbol{k}^0 + \delta\boldsymbol{S}^{0^{\mathrm{T}}}[A]\boldsymbol{S}^L + \delta\boldsymbol{k}^{0^{\mathrm{T}}}[B]\boldsymbol{S}^L\\
&+ \sum_m \delta\boldsymbol{S}^{0^{\mathrm{T}}}[\overline{E}^m]\boldsymbol{E}^m + \sum_m \delta\boldsymbol{k}^{0^{\mathrm{T}}}[\widehat{E}^m]\boldsymbol{E}^m + \sum_m \delta\boldsymbol{S}^{L^{\mathrm{T}}}[\overline{E}^m]\boldsymbol{E}^m \Big)\,\mathrm{d}A\\
&+ \int_{\Gamma_\tau} \delta\bar{\boldsymbol{u}}^{\mathrm{T}}\bar{\boldsymbol{\tau}}\,\mathrm{d}\Gamma = 0,\\
\delta\boldsymbol{\varphi}^{\mathrm{T}}\boldsymbol{\Psi}_e = -\int_{A_0} &\Big(\sum_m \delta\boldsymbol{E}^{m^{\mathrm{T}}}[\overline{E}^m]\boldsymbol{S}^0 + \sum_m \delta\boldsymbol{E}^{m^{\mathrm{T}}}[\widehat{E}^m]\boldsymbol{k}^0 + \sum_m \delta\boldsymbol{E}^{m^{\mathrm{T}}}[\overline{E}^m]\boldsymbol{S}^L + \sum_{mn} \delta\boldsymbol{E}^{m^{\mathrm{T}}}[G^{mn}]\boldsymbol{E}^n \Big)\,\mathrm{d}A\\
&+ \int_{\Gamma_q} \delta\bar{\boldsymbol{\varphi}}^{\mathrm{T}}\bar{\boldsymbol{q}}\,\mathrm{d}\Gamma = 0, \quad m,n = 1,\ldots,N
\end{aligned} \tag{6}$$

The first equation describes the mechanical equilibrium of an active laminate, where the first line contains linear stiffness terms, the second nonlinear stiffness terms and the third linear and nonlinear piezoelectric terms. The second equation describes the electrical (sensory) equilibrium of the piezoelectric laminate at a state (u, φ). In these equations, A_0 is the mid-surface; A, B, D are equivalent in-plane stiffness matrices, A_S is the shear stiffness matrix; $\overline{E}^m$, $\widehat{E}^m$ are in-plane and out-of-plane laminate piezoelectric matrices, and G^{mn} are electric permittivity matrices of the laminate (Saravanos, 1997).

Eq. (6) eventually provide a set of coupled nonlinear equations which govern the buckling response of piezoelectric laminates. Eq. (6) may not be solved directly, but they form the basis for the development of various iterative or searching solution techniques. The Newton–Raphson technique was chosen in this work due to its simplicity, but also because it provides a linearized system of equations of motion. In this context, Eq. (6) are further differentiated to yield

$$\begin{aligned}
\delta \boldsymbol{u}^{\mathrm{T}}\, \mathrm{d}\boldsymbol{\Psi}_u = & -\int_{A_0} \Big(\delta \boldsymbol{S}^{0^{\mathrm{T}}} [A]\, \mathrm{d}\boldsymbol{S}^0 + \delta \boldsymbol{S}^{0^{\mathrm{T}}} [B]\, \mathrm{d}\boldsymbol{k}^0 + \delta \boldsymbol{k}^{0^{\mathrm{T}}} [B]\, \mathrm{d}\boldsymbol{S}^0 + \delta \boldsymbol{k}^{0^{\mathrm{T}}} [D]\, \mathrm{d}\boldsymbol{k}^0 + \delta \boldsymbol{S}^{0^{\mathrm{T}}} [A_{\mathrm{S}}]\, \mathrm{d}\boldsymbol{S}^0 \\
& + \delta \boldsymbol{S}^{L^{\mathrm{T}}} [A]\, \mathrm{d}\boldsymbol{S}^0 + \delta \boldsymbol{S}^{L^{\mathrm{T}}} [A]\, \mathrm{d}\boldsymbol{S}^L + \delta \boldsymbol{S}^{L^{\mathrm{T}}} [B]\, \mathrm{d}\boldsymbol{k}^0 + \delta \boldsymbol{S}^{0^{\mathrm{T}}} [A]\, \mathrm{d}\boldsymbol{S}^L \\
& + \delta \boldsymbol{k}^{0^{\mathrm{T}}} [B]\, \mathrm{d}\boldsymbol{S}^L + \mathrm{d}\delta \boldsymbol{S}^{L^{\mathrm{T}}} [A] \boldsymbol{S}^L + \mathrm{d}\delta \boldsymbol{S}^{L^{\mathrm{T}}} \boldsymbol{N} + \sum_m \delta \boldsymbol{S}^{0^{\mathrm{T}}} [\overline{E}^m]\, \mathrm{d}\boldsymbol{E}^m \\
& + \sum_m \delta \boldsymbol{k}^{0^{\mathrm{T}}} [\widehat{E}^m]\, \mathrm{d}\boldsymbol{E}^m_{\mathrm{S}} + \sum_m \delta \boldsymbol{S}^{L^{\mathrm{T}}} [\overline{E}^m]\, \mathrm{d}\boldsymbol{E}^m \Big) \mathrm{d}A, \\
\delta \boldsymbol{\varphi}^{\mathrm{T}}\, \mathrm{d}\boldsymbol{\Psi}_e = & -\int_{A_0} \left(\sum_m \delta \boldsymbol{E}^{m^{\mathrm{T}}} [\overline{E}^m]\, \mathrm{d}\boldsymbol{S}^0 + \sum_m \delta \boldsymbol{E}^{m^{\mathrm{T}}} [\widehat{E}^m]\, \mathrm{d}\boldsymbol{k}^0 + \sum_m \delta \boldsymbol{E}^{m^{\mathrm{T}}} [\overline{E}^m]\, \mathrm{d}\boldsymbol{S}^L + \sum_{mn} \delta \boldsymbol{E}^{m^{\mathrm{T}}} [G^{mn}]\, \mathrm{d}\boldsymbol{E}^n \right) \mathrm{d}A
\end{aligned} \tag{7}$$

where δ expresses the variation of state variables u and φ. The term with the average in-plane stress vector $\boldsymbol{N}$ of the piezoelectric laminate appearing in Eq. (7) represents the stress stiffening effects. The average stress has the form

$$N_i = [A_{ij}] S^0_j + [B_{ij}] k^0_j - \sum_{m-1}^{N} [\overline{E}^m_{3i}] E^m_3, \quad i, j = 1, 2, 6 \tag{8}$$

By observing Eq. (8), the two right hand side terms represent respectively the average mechanical stress components due to extension and extension–flexure coupling for unsymmetric plates, while the third term represents the average piezoelectric stresses.

3. Finite element formulation

A finite element methodology for the buckling and postbuckling analysis of composite piezoelectric plates is formulated, encompassing the previous generalized nonlinear laminate mechanics. The state variables are approximated on the reference mid-plane A_0 with local interpolation functions of the following form

$$\begin{aligned}
\boldsymbol{u}_j^0(x,y,t) &= \sum_{i=1}^{M} \boldsymbol{u}_j^{0i}(t)\boldsymbol{P}^i(x,y), \quad j=1,\ldots,3,\\
\boldsymbol{\beta}_j^0(x,y,t) &= \sum_{i=1}^{M} \boldsymbol{\beta}_j^i(t)\boldsymbol{P}^i(x,y), \quad j=1,\ldots,2,\\
\boldsymbol{\varphi}_j^m(x,y,t) &= \sum_{i=1}^{M} \boldsymbol{\varphi}^{mi}(t)\boldsymbol{P}^i(x,y), \quad j=1,\ldots,N
\end{aligned} \tag{9}$$

where M is the number of element nodes, $\boldsymbol{P}^i$ are in-plane shape functions, superscript i indicates nodal degrees of freedom, which include mid-plane displacements $\boldsymbol{u}^0$, rotations $\boldsymbol{\beta}$ and electric potential $\boldsymbol{\varphi}^m$; N indicates the number of unknown electric potential values describing the layerwise representation through the laminate thickness. Thus a family of in-plane elements is defined with five structural and N electric degrees of freedom per node.

Combining Eq. (4) with Eq. (9), substituting into Eq. (6) and collecting the common nodal displacement and electric potential terms, the following coupled system of equations results

$$\begin{aligned}
\boldsymbol{\Psi}_u(u,\varphi) &= -[K_{uu}(u,\varphi)]\boldsymbol{u} - [K_{ue}(u,\varphi)]\boldsymbol{\varphi} + \boldsymbol{F},\\
\boldsymbol{\Psi}_e(u,\varphi) &= -[K_{eu}(u,\varphi)]\boldsymbol{u} - [K_{ee}(u,\varphi)]\boldsymbol{\varphi} + \boldsymbol{Q}
\end{aligned} \tag{10}$$

which may contain the nodal displacement $\{u\}$ and electric potential $\{\varphi\}$ vectors as unknowns. The nodal electric potential vector $\boldsymbol{\varphi} = \{\boldsymbol{\varphi}^{\mathrm{A}}, \boldsymbol{\varphi}^{\mathrm{S}}\}$ encompasses both active and sensory electric potential terms, where $\boldsymbol{\varphi}^{\mathrm{A}}$ and $\boldsymbol{\varphi}^{\mathrm{S}}$ are vectors including the applied nodal electric potentials at the actuators and the free nodal electric potentials at the sensors, respectively. The matrices $[K]$ with subscripts uu, ue, ee indicate the actual nonlinear stiffness, piezoelectric and permittivity matrices of the plate. $\boldsymbol{F}$ and $\boldsymbol{Q}$ are the externally applied loads and charge vectors respectively. At the point of mechanical and electrical equilibrium ($\boldsymbol{\Psi}_u(u^*,\varphi^*) = \boldsymbol{\Psi}_e(u^*,\varphi^*) = 0$), the previous equations provide a discrete system of nonlinear equations. Away from the equilibrium point, the first equation yields the nodal imbalance force vector $\boldsymbol{\Psi}_u$ between internal forces, piezoelectric forces, and externally applied mechanical loads; whereas, the second equation yields the imbalance charge vector $\boldsymbol{\Psi}_e$ between piezoelectric charges, internal charges and externally applied charges. The actual structural, piezoelectric and permittivity matrices are expressed more analytically by the following equations

$$\begin{aligned}
[K_{uu}(u,\varphi)] &= [K_{uu}^0] + [K_{uu}^L] + [K_{uu}^0] + [P_1(\boldsymbol{u})]/2 + [P_2(\boldsymbol{u}^2)]/3,\\
[K_{ue}(u,\varphi)] &= [K_{ue}^0] + [K_{ue}^L] + [K_{ue}^0] + [P_3(\boldsymbol{u})],\\
[K_{eu}(u,\varphi)] &= [K_{eu}^0] + [K_{eu}^L] = [K_{eu}^0] + [P_4(\boldsymbol{u})]/2,\\
[K_{ee}(u,\varphi)] &= [K_{ee}^0]
\end{aligned} \tag{11}$$

where superscripts 0 and L indicate linear and nonlinear components; $P_1(\boldsymbol{u})$ and $P_2(\boldsymbol{u}^2)$ indicate known nonlinear stiffness terms which respectively depend linearly and quadratically on displacements. $P_3(\boldsymbol{u})$ and $P_4(\boldsymbol{u})$ are new terms indicating, respectively, the nonlinear part of the piezoelectric matrices which both depend linearly on displacements. As seen in Appendix A, the matrix $P_3(\boldsymbol{u})$ appears in piezolaminates having unsymmetrically placed actuators, when the latter are deformed at high rotation angles $w_{,x}$, $w_{,y}$. When multiplied by the applied electric potential, the term yields a nonlinear actuator force component acting through the thickness direction z; the effect of this term is illustrated in the "numerical results" section. Similarly, the term $P_4(\boldsymbol{u})$ when multiplied by the displacement vector, represents nonlinear electric charges at piezoelectric layers during high deformation angles. The solution of the nonlinear system (10) is calculated iteratively using the Newton-Raphson method. Substituting Eq. (4) together with Eq. (9) into Eq. (7) and after collecting the common terms, the linearized matrices for the nonlinear piezoelectric

structure are obtained. These, in the context of a Newton–Raphson method provide a coupled system of equations

$$[\overline{K}_{uu}(u,\varphi)]\,\mathrm{d}\boldsymbol{u} + [\overline{K}_{ue}(u,\varphi)]\,\mathrm{d}\boldsymbol{\varphi}^S = \boldsymbol{\Psi}_u(u,\varphi), \qquad [\overline{K}_{eu}(u,\varphi)]\,\mathrm{d}\boldsymbol{u} + [\overline{K}_{ee}]\,\mathrm{d}\boldsymbol{\varphi}^S = \boldsymbol{\Psi}_e(u,\varphi) \tag{12}$$

which yields a step $(\mathrm{d}\boldsymbol{u}, \mathrm{d}\boldsymbol{\varphi}^S)$ towards the solution $(\boldsymbol{u}^*, \boldsymbol{\varphi}^*)$ of the nonlinear equations (10). The first equation describes the linearized buckling behavior of an adaptive structure including actuator input, while the second equation describes the linearized sensory response about a point (u,φ) during buckling.

The tangential structural, piezoelectric and permittivity matrices contain the following terms

$$\begin{aligned}
&[\overline{K}_{uu}(u,\varphi)] = [\overline{K}^0_{uu}] + [\overline{K}^\sigma_{uu}] + [\overline{K}^L_{uu}] = [\overline{K}^0_{uu}] + [\overline{K}^\sigma_{uu}] + [P_1(\boldsymbol{u})] + [P_2(\boldsymbol{u}^2)],\\
&[\overline{K}_{ue}(u,\varphi)] = [\overline{K}^0_{ue}] + [\overline{K}^L_{ue}] = [\overline{K}^0_{ue}] + [P_3(\boldsymbol{u})],\\
&[\overline{K}_{eu}(u,\varphi)] = [\overline{K}^0_{eu}] + [\overline{K}^L_{eu}] = [\overline{K}^0_{eu}] + [P_4(\boldsymbol{u})],\\
&[\overline{K}_{ee}(u,\varphi)] = [\overline{K}^0_{ee}]
\end{aligned} \tag{13}$$

The tangential matrices have very similar structure and terms with the actual system matrices in Eq. (11). However, there is a new matrix appearing, which is the stress stiffness matrix K^σ_{uu}, which includes the effect of linear stress on the tangential stiffness matrix. More detailed definitions of the total and tangential matrices are provided in Appendix A.

Linear buckling: The case of linear buckling of adaptive structures can be derived as a special case of Eq. (12) by neglecting the nonlinear tangential terms in Eq. (12) and assuming equilibrium. Solution of the resultant eigenproblem yields the critical buckling loads and corresponding buckling shapes (Varelis and Saravanos, 2002a,b).

4. Numerical results and discussion

In this section, validations and evaluations of the developed models are presented for various active and sensory piezoelectric composite beams and plates. Aluminum, Graphite–Epoxy composite, PZT5 piezoceramic and PVDF piezopolymer materials were considered with properties shown in Table 1. The location of piezoelectric layers in the piezolaminate is indicated with letter p using standard laminate notation. In the following examples we use the terms: ''critical buckling load'' to imply buckling loads predicted using linear buckling analysis; ''buckling'' to describe the complete phenomenon; and ''prebuckling'' and ''postbuckling'' to describe the range of the buckling response before and after the critical load, respectively.

4.1. Mechanical buckling of plates

A rectangular Gr/Epoxy $[\pm 45/0_2/\pm 45/0_2/\pm 45/0/90]_S$ panel subject to a combination of clamped-free and simple-supports and progressively loaded with an in-plane compressive line force applied along the free edge (see Fig. 2) was modeled. The dimensions of the panel were $L_x = 508$ mm, $L_y = 178$ mm and the thickness of each composite ply was $h_l = 0.14$ mm. The buckling response of the plate was measured by Starnes and Rouse (1981), and was also analyzed by Engelstad et al. (1992) using a shell element and assuming a doubly sinusoidal geometric imperfection in the panel shape. Linear buckling analysis using the present finite element predicted a critical buckling load $P_{\mathrm{cr}} = 45.066$ KN for the $(2,1)$ buckling mode. The buckling and postbuckling response was subsequently predicted for an increasing in-plane compressive mechanical force applied at the free edge. During the present analysis, a low doubly sinusoidal $(2,1)$ pressure was initially applied and remained constant during the in-plane loading, such that the resultant doubly sinusoidal transverse deformation $w_0/h = 4\%$ was within the range of initial geometrical

Table 1
Mechanical properties ($\varepsilon_0 = 8.85 \pm 10^{-12}$ F/m, electric permittivity of air)

Property	Gr/Epoxy	Al	PZT5	PVDF
Elastic properties				
E_{11} (GPa)	132.4	66	62	4
E_{22} (GPa)	10.8	66	62	4
G_{23} (GPa)	3.6	27	18	1.54
G_{13} (GPa)	5.6	27	23.6	1.54
G_{12} (GPa)	5.5	27	23.6	1.54
v_{12}	0.24	0.3	0.31	0.3
v_{13}	0.24	0.3	0.31	0.3
v_{23}	0.49	0.3	0.31	0.3
Piezoelectric coefficients (10^{-12} m/V)				
d_{31}	0	0	−220	−23
d_{32}	0	0	−220	−23
d_{24}	0	0	670	670
d_{15}	0	0	670	670
Electric permittivity				
$\varepsilon_{11}/\varepsilon_0$	3.5	3.5	2598	12.43
$\varepsilon_{22}/\varepsilon_0$	3	3	2598	12.43
$\varepsilon_{33}/\varepsilon_0$	3	3	2598	12.43
Mass density				
ρ (Kg/m^3)	1586	2768	2598	1000

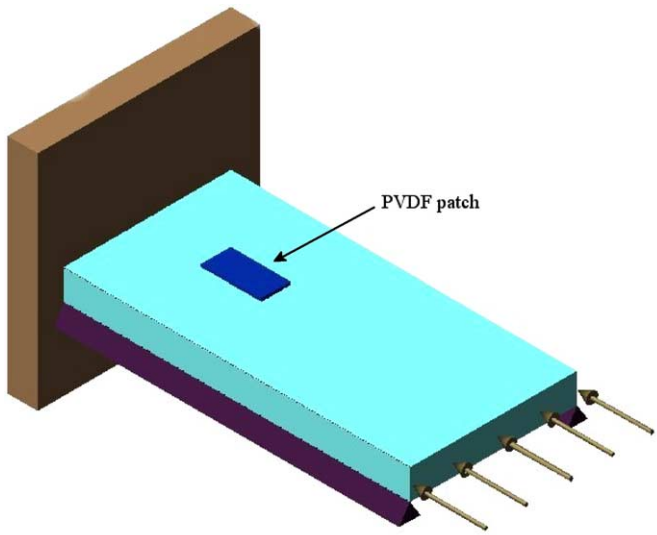

Fig. 2. Schematic composite plate configuration with two clamped sides, two simply supporting guides and an axial compressive load applied on one clamped side.

imperfection considered by Engelstad et al. (1992). The applied pressure may by considered as a comparable form of load imperfection which rendered the buckling response into a stable buckling path, similar to the one observed experimentally. Fig. 3 shows the predicted normalized transverse displacement at point

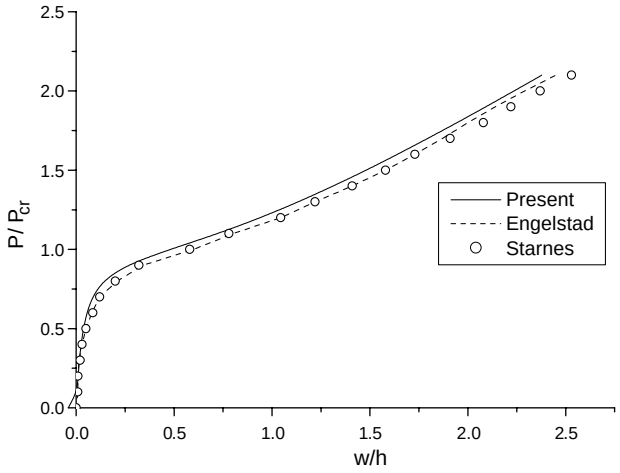

Fig. 3. Transverse deflection at point ($x = L_x/4$, $y = L_y/2$) of the $[\pm 45/0_2/\pm 45/0_2/\pm 45/0/90]_S$ composite plate shown in Fig. 2.

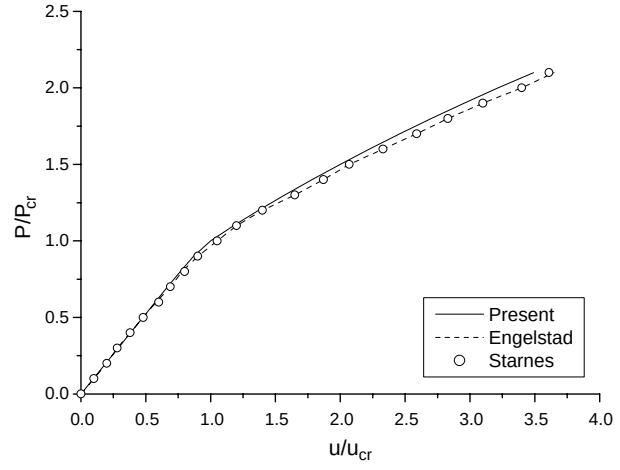

Fig. 4. Axial displacement at the loaded edge of the $[\pm 45/0_2/\pm 45/0_2/\pm 45/0/90]_S$ plate shown in Fig. 2.

($x = L_x/4$, $y = L_y/2$), while Fig. 4 shows the axial displacement at the loaded edge normalized by the axial displacement at the critical buckling load. The present predictions are in very good agreement with both reported numerical (Engelstad et al., 1992) and experimental results (Starnes and Rouse, 1981), which lends credence to the convergence and accuracy of the present mechanics and finite element.

Two $42.3 \times 29.6 \times 0.1$ mm piezopolymer PVDF sensor patches were also considered, each attached on the upper and lower surface of the plate approximately at point ($x = L_x/6$, $y = L_y/2$), with the upper terminals being free while the lower terminals were grounded. In order to realistically model the sensory response of the piezopatch, equality constrains were imposed on the nodal electric potential over the free terminal of each PVDF sensor using a penalty method, thus forcing the resultant sensory voltage over the terminal area to have the same value. Fig. 5 shows the predicted electric sensory potential produced by each sensor for the assumed polarity. Both sensors yield low and similar electric signals during prebuckling which begin to drastically differ in the buckling and postbuckling range, moreover, the predicted sensor signals follow the

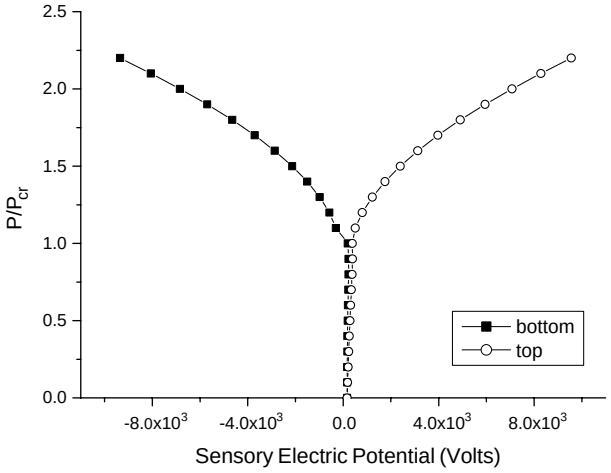

Fig. 5. Predicted electric potential at PVDF sensors during buckling and postbuckling attached on the upper and lower surface at point ($x = L_x/6$, $y = L_y/2$) of the $[\pm 45/0_2/\pm 45/0_2/\pm 45/0/90]_S$ plate.

trends of measured strains (Starnes and Rouse, 1981). The results demonstrate the inherent capability of the method to predict the response of piezoelectric sensors during buckling and postbuckling, yet, they also indicate the possibility of properly configured piezosensors to detect the onset of buckling and postbuckling in a smart plate structure.

4.2. Active structures

4.2.1. Active beam

The piezoelectric buckling and postbuckling of a [p/Al/p] clamped–clamped beam was examined. The beam was 200 mm long and 20 mm wide, the thickness of the Aluminum layer was 0.5 mm and of each PZT5 layer was 0.25 mm. Opposite electric potentials φ^A and $-\varphi^A$ volts (see Fig. 6a) were applied on the outer terminals of the upper and lower piezoactuator respectively, such that an in-plane compressive stress was effectively induced. In this manner, sufficiently high electric fields may cause a new type of buckling, termed thereafter "active" or "piezoelectric" buckling. The predicted critical electric potential is shown in Table 2. Fig. 7 shows the predicted normalized deflection at the center of the beam as function of the applied actuator voltage for the cases of perfect and imperfect active buckling. In the fist case, an unstable buckling path was predicted where the transverse deflection remained zero until the critical buckling electric potential was reached, and beyond this point a transverse deflection is initiated due to nonlinear matrices $[K^L]$. In the second case, an imperfection induced by a very low constant uniform pressure (1.2 Pa) was considered, thus stimulating the onset of a stable buckling path. In the prebuckling range, the transverse deflection increases rapidly as the applied electric potential induces a negative stress stiffness matrix $[K^\sigma]$, while near the critical point, the contribution of the nonlinear matrices begin to dominate the overall stiffness and the beam response passes through an inflection point into the postbuckling equilibrium state.

4.2.2. Active plate

The buckling response of an active square (200×200 mm) Gr/Epoxy-PZT5 $[p/0/90]_S$ plate, simply supported in all sides was predicted. The composite ply and piezolayer thicknesses were $h_l = 0.125$ mm and $h_p = 0.25$ mm, respectively. The polarities of the applied electric fields were the same as in the previous case (Fig. 6a), such that a biaxial in-plane piezoelectric force was induced. The predicted critical buckling electric

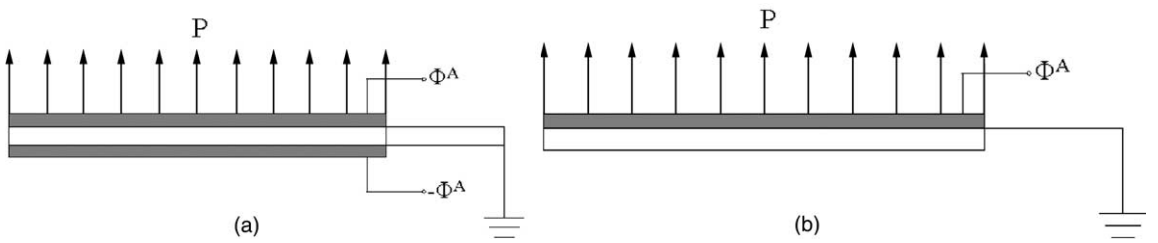

Fig. 6. Side view of actuator and applied electric potential configurations: (a) composite beam or plate with symmetric continuous piezoelectric actuators attached on upper and lower surface; (b) composite beam or plate side view with an asymmetric piezoelectric actuator attached on the upper surface.

Table 2
Predicted critical buckling electric potentials for active beams

Beam configuration	Critical electric potentials Φ_{cr} (V)
[p/Al/p]	188
[Al/p]	94

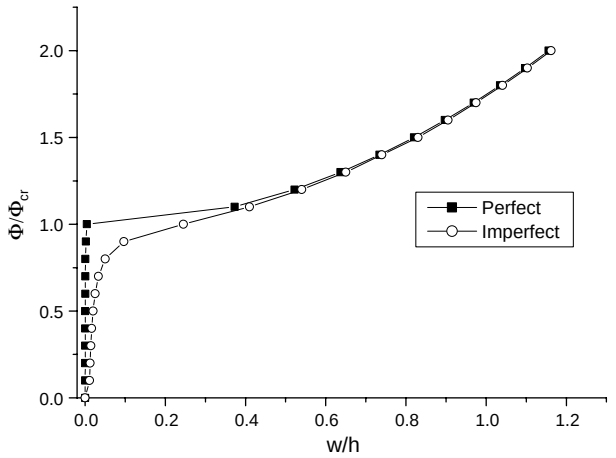

Fig. 7. Effect of an imperfection on piezoelectric buckling and postbuckling deflection at the center of a [p/Al/p] clamped–clamped active strip with unipolar electric fields applied at actuators (Fig. 6a).

potential, using linear buckling assumptions, is shown in Table 3. Fig. 8 shows the predicted normalized center transverse deflection of the plate for two cases: (a) considering only the linear initial stress matrix $[K^{\sigma}]$ component in Eq. (12), such that, the plate transits to the second buckling mode beyond the first critical buckling load; and (b) considering both the initial stress $[K^{\sigma}]$ and the nonlinear stiffness $[K^{L}]$ components, thus solving the nonlinear buckling problem. In this and the following two imperfect plate cases, a very low constant uniform pressure (4 Pa) was also considered. Clearly, the inclusion of the nonlinear terms enables the prediction of the postbuckling response.

Table 3
Predicted critical buckling electric potentials for active plates

Plate configuration	Critical electric potentials Φ_{cr} (V)
$[p/0/90]_S$	340.1
$[p/45/-45]_S$	206.6
[p/0/90/45/−45/p]	251.2
$[p/0/90/45/-45]_S$ (25% patch coverage)	1053.13
$[p/0/90/45/-45]_S$ (56% patch coverage)	859.75
$[p/0/90/45/-45]_S$ (100% patch coverage)	775
[0/90/45/−45/p]	209.2

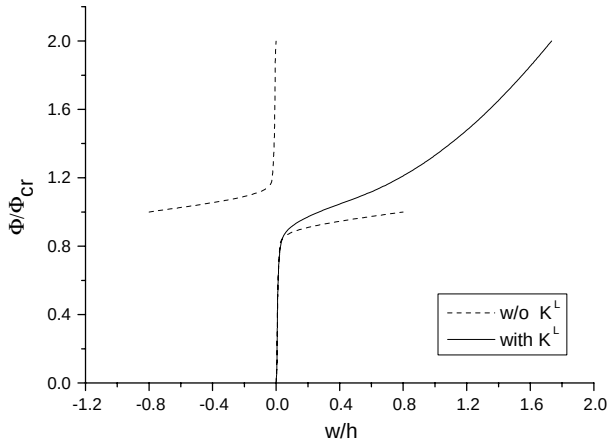

Fig. 8. Piezoelectric buckling and postbuckling deflection at the center of a $[p/0/90]_S$ simply-supported active plate with unipolar electric fields applied at the actuators (Fig. 6a).

4.2.3. Active laminated plates

The active buckling responses of three simply-supported active Gr/Epoxy plates with continuous PZT5 layers on their top and bottom surfaces and various laminations were considered. The dimensions were the same as in the previous case. The piezolayer thickness was $h_p = 0.25$ mm. The composite core laminations were $[0/90]_S$, $[45/-45]_S$ and [0/90/45/−45], all having same thicknesses equal to $h_c = 0.5$ mm. Identical unipolar electric fields with the previous case (Fig. 6a) were applied in all three plates. Fig. 9a shows the predicted transverse deflection at the center of each active plate without considering any imperfections. The electric potentials are normalized by the corresponding predicted critical values shown in Table 3. The plates with symmetric laminations follow an unstable bifurcation path, whereas, the [0/90/45/−45] plate follows a stable buckling and postbuckling path due to extension/bending coupling induced by the unsymmetric lamination. Fig. 9b shows the predicted center transverse deflection of each plate versus the applied voltage when an imperfection induced by a very low constant uniform pressure (5 Pa) was considered. In all cases, the postbuckling response is produced by the same mechanisms as discussed in the previous cases for beams and plates. However, it is noted that in the unsymmetric piezolaminate, additional membrane bending coupling terms contributed to the $P_1(\boldsymbol{u})$ stiffness matrix due to the laminate coupling matrix $[B]$.

4.2.4. Plates with actuator patches

The active buckling response of three square Gr/Epoxy-PZT5 $[p/0/90/45/-45]_S$ plates (200×200 mm), simply supported in all sides with 8 piezoceramic patches attached on the upper and lower surface as shown

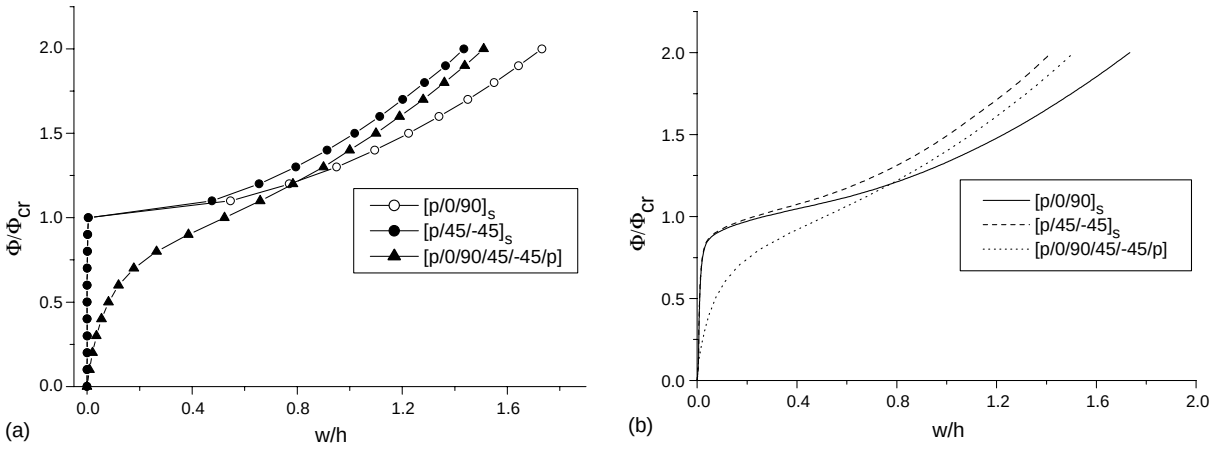

Fig. 9. Buckling and postbuckling deflection at the center of simply-supported active plates with various laminations, induced by unipolar electric fields at the actuators: (a) without imperfections; (b) with a pressure imperfection considered.

in Fig. 10a, was predicted. The piezoceramic patch coverage of each piezolaminate was 25%, 56% and 100% of the plate area, the latter representing the case of a continuous layer. The composite and piezoelectric ply thicknesses were $h_l = 0.125$ mm and $h_p = 0.25$ mm respectively. The patches were subject to unipolar electric fields by applying opposite electric potential on the upper and lower outer terminals, as shown in Fig. 10b. A very low uniform pressure (5 Pa) was also applied. The predicted critical electric potentials for

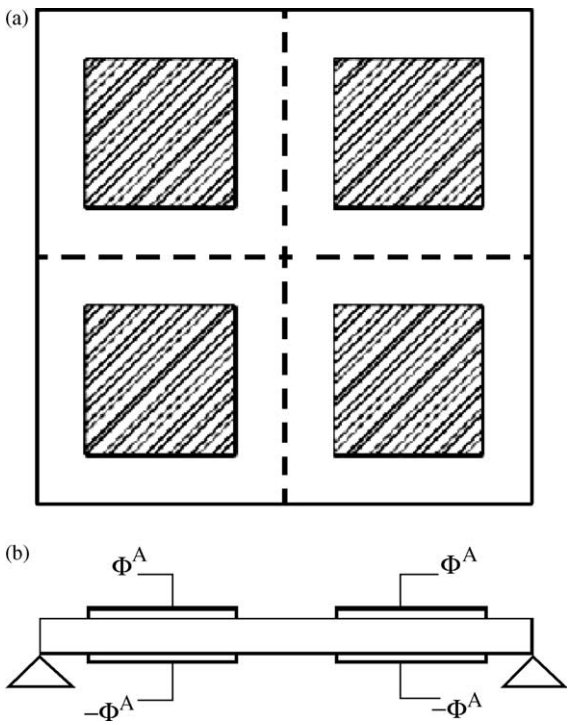

Fig. 10. Schematic configuration of plate with piezoelectric patches attached on upper and lower surface: (a) top, and (b) side view.

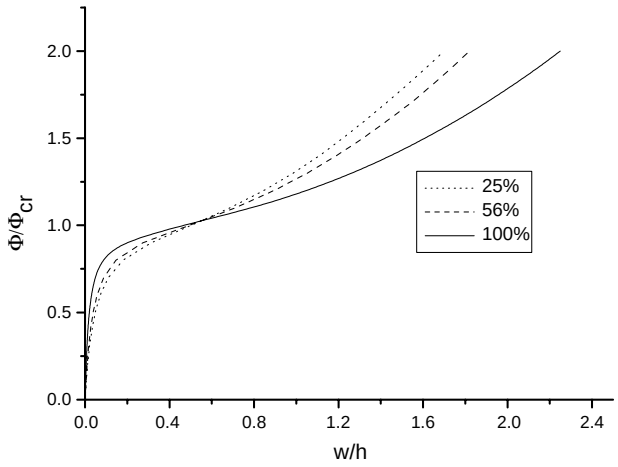

Fig. 11. Buckling deflection at the center of a $[p/0/90/45/-45]_S$ simply-supported plate induced by PZT5 actuator patches of various coverages.

each case are shown in Table 3. Due to symmetry, a quarter of the plate was modeled. Fig. 11 shows the deflection (normalized by the total thickness of the composite laminate). The diagram shows that the piezolaminate with the lower actuator coverage, is driven more rapidly into the postbuckling region due to its lower stiffness, however a higher buckling electric field is required. The higher contribution of the nonlinear stiffness component in the postbuckling regime of the plate with the lower actuator coverage (25%) is also shown in Fig. 11.

4.2.5. Beam with asymmetric actuation

The active response of a hinged–hinged asymmetric [Al/p] beam $L_x = 200$ mm, $L_y = 20$ mm, with a single PZT5 layer attached on the upper surface was predicted. The thickness of the Aluminum was 0.75 mm and of the piezolayer 0.25 mm. An electric voltage φ^A was imposed on the upper terminal while the inner terminal remained grounded as shown in Fig. 6b, thus both in-plane and bending loads were induced by the actuator. The predicted critical electric potential is shown in Table 2.

One of the objectives of this example is to quantify the effect of the term $K_{ue}^L = P_3(\boldsymbol{u})$, which is seemingly the more important of the two nonlinear piezoelectric components appearing in Eqs. (11) and (13), as it affects the actuator performance and consequently the active buckling behavior. It is recalled, that this term attains nonzero values in laminates with asymmetric actuator configurations deformed at high rotation angles $w_{,x}$, $w_{,y}$, and represents an active nonlinear force component acting along the thickness direction z. Fig. 12 shows the center deflection of the active beam versus the applied electric potential for the cases where the piezoelectric matrix includes: (a) only the linear piezoelectric term K_{ue}^0, and (b) both linear K_{ue}^0 and nonlinear $P_3(\boldsymbol{u})$ piezoelectric matrices. In both cases, the induced stress by the piezoactuator results in a bending moment and a compressive in-plane force, causing the stable transverse deflection path seen in Fig. 12 for $P_3(\boldsymbol{u}) = 0$. The difference predicted with the inclusion of $P_3(\boldsymbol{u})$, however, represents the significant effect on the buckling response of an active force acting transversely to the beam at high rotation angles.

4.2.6. Hinged plate with asymmetric actuator

The case of a fully hinged asymmetric [0/90/45/−45/p] active plate with a continuous piezoelectric active layer attached on the upper surface was examined. The dimensions of the plate were identical to those in the previous cases. The thickness of each Gr/Epoxy ply was 0.25 mm and of the PZT5 layer 0.25 mm. This is

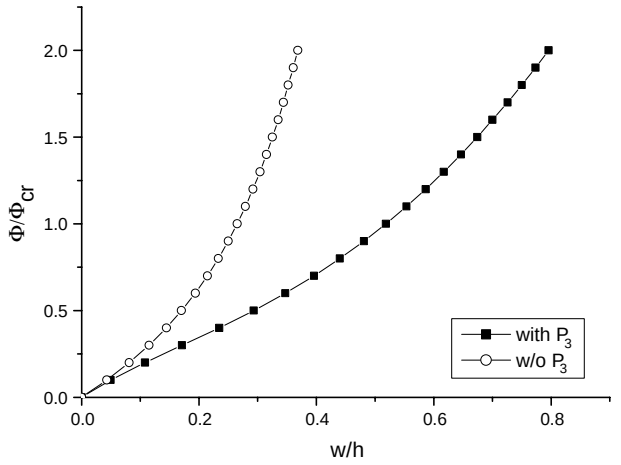

Fig. 12. Transverse center deflection of a hinged–hinged active asymmetric [Al/p] strip induced by a single continuous actuator attached on the upper surface (Fig. 6b).

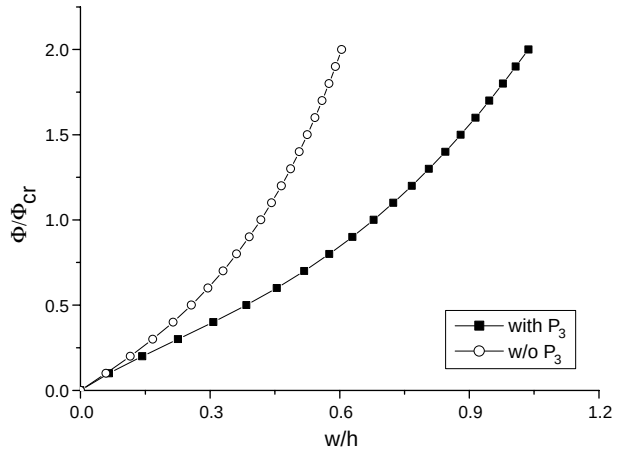

Fig. 13. Transverse center deflection of a fully hinged [0/90/45/−45/p] asymmetric plate induced by continuous actuator attached on the upper surface (Fig. 6b).

seemingly the most complex case considered thus far, involving all terms included in the present mechanics due to the asymmetries in both laminate and actuator configuration. Table 3 shows the predicted critical electric potential. Fig. 13 shows the center deflection of the plate as function of the applied actuator voltage with and without consideration of the nonlinear piezoelectric matrix $P_3(\boldsymbol{u})$. The discussion of the previous case regarding the effect of $P_3(\boldsymbol{u})$ applies also here. As in the previous case, the absence of $P_3(\boldsymbol{u})$ component may result in significant underestimation of the active buckling response.

4.3. Electromechanical buckling and active buckling compensation

4.3.1. Beams

In this case the buckling and postbuckling response of a hinged–hinged, 200 mm long and 20 mm wide [p/Al/p] beam, subject to a combination of electromechanical loading was investigated. The thickness of

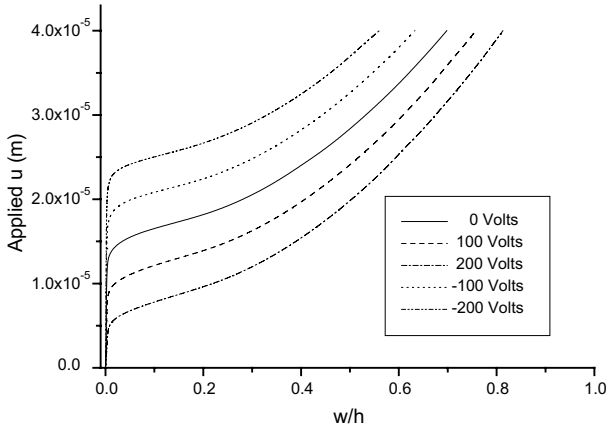

Fig. 14. Transverse center deflection during electromechanical buckling of a hinged–hinged [p/Al/p] symmetric beam with continuous piezoactuators induced by combined in-plane displacement applied at free edge and electric potential φ^{A} at actuators (Fig. 6a).

the Aluminum layer was 1.5 mm and of each PZT5 layer was 0.25 mm. An increasing mechanical axial compressive displacement was imposed on one hinged edge combined with electric potential applied on the actuators as shown in Fig. 6a. A constant uniform pressure of 4 Pa was also applied to induce a stable buckling path. The predicted critical mechanical compressive displacement, for the case of 0 V applied on the actuators, was $u_{cr} = 5 \times 10^{-6}$ m. Fig. 14 shows the normalized center deflection of the beam in the buckling and postbuckling region for various values of applied electric voltages. Clearly, the transverse displacement is directly related to the applied electric potential on the actuators. Interestingly, the curves of the graph corresponding to negative values of applied potentials indicate that the plate will enter into a buckling path under higher mechanical force values, and quantify the possibility to actively compensate mechanical buckling by inducing tensile average stresses with the piezoactuators. Whereas, the curves of the graph corresponding to positive values, indicate a range of high buckling risk, since the beam is predicted to enter into a buckling path under a combination of lower in-plane forces and positive electric potentials, both inducing compressive in-plane stresses. Both cases are unique to smart piezoelectric structures and entail their own technical merit, moreover, both examples highlight the predictive capabilities and quality of the present formulation.

4.3.2. Plates

The active electromechanical buckling behavior of a square (200×200 mm) Gr/Epoxy $[p/45/-45]_S$ plate having both edges perpendicular to the x-axis clamped was finally investigated. The thickness of each composite ply was 0.5 mm and of each piezolayer 0.25 mm. An increasing mechanical in-plane compressive displacement along the x-axis was imposed on one clamped edge combined with unipolar electric fields applied on the active layers as shown in Fig. 6a. A constant uniform pressure of 2.5 Pa was also considered. The predicted critical mechanical compressive displacement, for the case of 0 V, was $u_{cr} = 0.12 \times 10^{-4}$ m. Fig. 15 shows the normalized transverse deflection of the plate in the pre- and postbuckling region. The results quantify the possibility of mitigating or increasing buckling risk depending on the applied polarity of actuator voltage, and most comments of the discussion in the previous paragraph apply also here. The results also suggest, that depending on the case, high electric fields may be required to be applied on the actuators in order to compensate buckling which may exceed the linear range of piezoelectric properties assumed in this work. While the presented results aim to quantify the sensitivity of mechanical buckling to

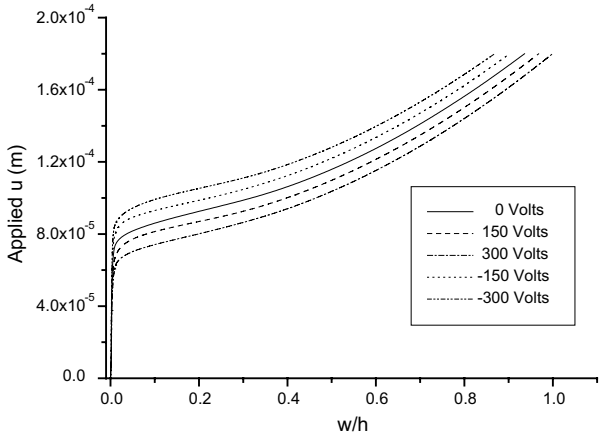

Fig. 15. Transverse center deflection during electromechanical buckling of an active $[p/45/-45]_S$ clamped–clamped plate induced by a combination of an applied axial displacement at one clamped end and uniform electric potential φ^A at the actuators (Fig. 6a).

applied actuator fields, the presented mechanics entails the structure to address nonlinear piezoelectric response in future work.

5. Summary and conclusions

A theoretical framework was presented for the coupled buckling and postbuckling analysis of piezoelectric adaptive plate structures with stress stiffening and geometric effects due to large rotations including a finite element based solution method. Based on this framework, an eight node nonlinear plate element was developed and encoded into a research code, enabling formal computational predictions of the buckling and postbuckling response of composite beams and plates with piezoelectric actuators. Numerical results were presented for various active beam and plate configurations and their buckling and postbuckling responses were predicted and analyzed. The case of active piezoelectric buckling induced by piezoactuators was also demonstrated and quantified. The effects of laminate configurations, actuator forms and unsymmetric actuation were also studied. The onset of a transverse active force/pressure component at large rotations resulting from nonlinear piezoelectric terms was predicted for the case of unsymmetric actuation, and its contribution on the transverse deflection was quantified. Finally the results quantified the capability range of piezocomposite structures to actively mitigate mechanical buckling and postbuckling with the application of proper electric fields on the actuators. Overall, the results illustrated the complexity and significance of active buckling and postbuckling behavior of piezoelectric adaptive structures, and highlighted the value and quality of the present nonlinear theory and finite element in the analysis and design of adaptive structures.

Acknowledgement

This work was partially funded through the Karatheodoris Program of the Research Office of the University of Patras. This support is gratefully acknowledged.

Appendix A

Nonlinear strains:

$$S_{L1} = \tfrac{1}{2} w^{0^2}_{,x}, \qquad S_{L2} = \tfrac{1}{2} w^{0^2}_{,y}, \qquad S_{L6} = w^0_{,x} \cdot w^0_{,y}$$

Electric field vector:

$$E_i(x,y,\zeta,t) = \sum_{m=1}^{N} E_i^m(x,y,t)\boldsymbol{\Psi}^m(\zeta), \quad i = 1,2$$

$$E_3(x,y,\zeta,t) = \sum_{m=1}^{N} E_3^m(x,y,t)\boldsymbol{\Psi}^m_{,\zeta}(\zeta)$$

Generalized electric field vector:

$$E_1^m = -\varphi^m_{,x}, \qquad E_2^m = -\varphi^m_{,y}, \qquad E_3^m = -\varphi^m$$

Tangential matrix components (Eq. (13)):

$$\delta\boldsymbol{u}^{\mathrm{T}}[\overline{K}^0_{uu}]\,\mathrm{d}\boldsymbol{u} = \int_{A_0} \left(\delta\boldsymbol{S}^{0^{\mathrm{T}}}[A]\,\mathrm{d}\boldsymbol{S}^0 + \delta\boldsymbol{S}^{0^{\mathrm{T}}}[B]\,\mathrm{d}\boldsymbol{k}^0 + \delta\boldsymbol{k}^{0^{\mathrm{T}}}[B]\,\mathrm{d}\boldsymbol{S}^0 + \delta\boldsymbol{k}^{0^{\mathrm{T}}}[D]\,\mathrm{d}\boldsymbol{k}^0 + \delta\boldsymbol{S}_{\mathrm{S}}^{0^{\mathrm{T}}}[A_{\mathrm{S}}]\,\mathrm{d}\boldsymbol{S}_{\mathrm{S}}^0\right)\mathrm{d}A$$

$$\delta\boldsymbol{u}^{\mathrm{T}}[\overline{K}^{\sigma}_{uu}]\,\mathrm{d}\boldsymbol{u} = \int_{A_0} \mathrm{d}\delta\boldsymbol{S}^{L^{\mathrm{T}}}\boldsymbol{N}\,\mathrm{d}A$$

$$\delta\boldsymbol{u}^{\mathrm{T}}[\overline{K}^{L}_{uu}]\,\mathrm{d}\boldsymbol{u} = \int_{A_0} \left(\delta\boldsymbol{S}^{L^{\mathrm{T}}}[A]\,\mathrm{d}\boldsymbol{S}^0 + \delta\boldsymbol{S}^{L^{\mathrm{T}}}[B]\,\mathrm{d}\boldsymbol{k}^0 + \delta\boldsymbol{S}^{0^{\mathrm{T}}}[A]\,\mathrm{d}\boldsymbol{S}^L + \delta\boldsymbol{k}^{0^{\mathrm{T}}}[B]\,\mathrm{d}\boldsymbol{S}^L\right)\mathrm{d}A$$

$$\delta\boldsymbol{u}^{\mathrm{T}}[\overline{K}^{L}_{uu}]\,\mathrm{d}\boldsymbol{u} = \int_{A_0} \left(\delta\boldsymbol{S}^{L^{\mathrm{T}}}[A]\,\mathrm{d}\boldsymbol{S}^L + \mathrm{d}\delta\boldsymbol{S}^{L^{\mathrm{T}}}[A]\boldsymbol{S}^L\right)\mathrm{d}A$$

$$\delta\boldsymbol{u}^{\mathrm{T}}[\overline{K}^{0}_{ue}]\,\mathrm{d}\boldsymbol{\varphi} = \int_{A_0} \left(\delta\boldsymbol{S}^{0^{\mathrm{T}}}[\overline{E}^m]\,\mathrm{d}\boldsymbol{E}^m + \delta\boldsymbol{k}^{0^{\mathrm{T}}}[\widehat{E}^m]\,\mathrm{d}\boldsymbol{E}^m\right)\mathrm{d}A$$

$$\delta\boldsymbol{u}^{\mathrm{T}}[\overline{K}^{L}_{ue}]\,\mathrm{d}\boldsymbol{\varphi} = \int_{A_0} \left(\delta\boldsymbol{S}^{L^{\mathrm{T}}}[\overline{E}^m]\,\mathrm{d}\boldsymbol{E}^m\right)\mathrm{d}A$$

$$\delta\boldsymbol{\varphi}^{\mathrm{T}}[\overline{K}^{0}_{eu}]\,\mathrm{d}\boldsymbol{u} = \int_{A_0} \left(\delta\boldsymbol{E}^{m^{\mathrm{T}}}[\overline{E}^m]\,\mathrm{d}\boldsymbol{S}^0 + \delta\boldsymbol{E}^{m^{\mathrm{T}}}[\widehat{E}^m]\,\mathrm{d}\boldsymbol{k}^0\right)\mathrm{d}A$$

$$\delta\boldsymbol{\varphi}^{\mathrm{T}}[\overline{K}^{L}_{eu}]\,\mathrm{d}\boldsymbol{u} = \int_{A_0} \left(\delta\boldsymbol{E}^{m^{\mathrm{T}}}[\overline{E}^m]\,\mathrm{d}\boldsymbol{S}^L\right)\mathrm{d}A$$

$$\delta\boldsymbol{\varphi}^{\mathrm{T}}[\overline{K}^{0}_{ee}]\,\mathrm{d}\boldsymbol{\varphi} = \int_{A_0} \left(\delta\boldsymbol{E}^{m^{\mathrm{T}}}[G^{mn}]\,\mathrm{d}\boldsymbol{E}^n\right)\mathrm{d}A$$

Actual matrix components (Eq. (11)):

$$\delta\boldsymbol{u}^{\mathrm{T}}[K^0_{uu}]\boldsymbol{u} = \int_{A_0} \left(\delta\boldsymbol{S}^{0^{\mathrm{T}}}[A]\boldsymbol{S}^0 + \delta\boldsymbol{S}^{0^{\mathrm{T}}}[B]\boldsymbol{k}^0 + \delta\boldsymbol{k}^{0^{\mathrm{T}}}[B]\boldsymbol{S}^0 + \delta\boldsymbol{k}^{0^{\mathrm{T}}}[D]\boldsymbol{k}^0 + \delta\boldsymbol{S}_{\mathrm{S}}^{0^{\mathrm{T}}}[A_{\mathrm{S}}]\boldsymbol{S}_{\mathrm{S}}^0\right)\mathrm{d}A$$

$$\delta \boldsymbol{u}^{\mathrm{T}}[K^{L}_{uu}]\boldsymbol{u} = \int_{A_0} \left(\delta \boldsymbol{S}^{L^{\mathrm{T}}}[A]\boldsymbol{S}^{0} + \delta \boldsymbol{S}^{L^{\mathrm{T}}}[B]\boldsymbol{k}^{0} + \delta \boldsymbol{S}^{0^{\mathrm{T}}}[A]\boldsymbol{S}^{L} + \delta \boldsymbol{k}^{0^{\mathrm{T}}}[B]\boldsymbol{S}^{L} \right) \mathrm{d}A$$

$$\delta \boldsymbol{u}^{\mathrm{T}}[K^{L}_{uu}]\boldsymbol{u} = \int_{A_0} \left(\delta \boldsymbol{S}^{L^{\mathrm{T}}}[A]\boldsymbol{S}^{L} \right) \mathrm{d}A$$

$$\delta \boldsymbol{u}^{\mathrm{T}}[K^{0}_{ue}]\boldsymbol{\varphi} = \int_{A_0} \left(\delta \boldsymbol{S}^{0^{\mathrm{T}}}[\overline{E}^{m}]\boldsymbol{E}^{m} + \delta \boldsymbol{k}^{0^{\mathrm{T}}}[\widehat{E}^{m}]\boldsymbol{E}^{m} \right) \mathrm{d}A$$

$$\delta \boldsymbol{u}^{\mathrm{T}}[K^{L}_{ue}]\boldsymbol{\varphi} = \int_{A_0} \left(\delta \boldsymbol{S}^{L^{\mathrm{T}}}[\overline{E}^{m}]\boldsymbol{E}^{m} \right) \mathrm{d}A$$

$$\delta \boldsymbol{\varphi}^{\mathrm{T}}[K^{0}_{eu}]\boldsymbol{u} = \int_{A_0} \left(\delta \boldsymbol{E}^{m^{\mathrm{T}}}[\overline{E}^{m}]\boldsymbol{S}^{0} + \delta \boldsymbol{E}^{m^{\mathrm{T}}}[\widehat{E}^{m}]\boldsymbol{k}^{0} \right) \mathrm{d}A$$

$$\delta \boldsymbol{\varphi}^{\mathrm{T}}[K^{L}_{eu}]\boldsymbol{u} = \int_{A_0} \left(\delta \boldsymbol{E}^{m^{\mathrm{T}}}[\overline{E}^{m}]\boldsymbol{S}^{L} \right) \mathrm{d}A$$

$$\delta \boldsymbol{\varphi}^{\mathrm{T}}[K^{0}_{ee}]\boldsymbol{\varphi} = \int_{A_0} \left(\delta \boldsymbol{E}^{m^{\mathrm{T}}}[G^{mn}]\boldsymbol{E}^{n} \right) \mathrm{d}A$$

References

Chia, C.Y., 1988. Geometrically nonlinear behavior of composite plates: a review. Applied Mechanics Reviews 41, 439–451.

de Faria, A.R., de Almeida, S.F.M., 1999. Enhancement of pre-buckling behavior of composite beams with geometric imperfections using piezoelectric actuators. Composites: Part B 30, 43–50.

Di Scuva, M., Icardi, U., 1995. Large deflection of adaptive multilayered Timoshenko beams. Composite Structures 31, 49–60.

Engelstad, S.P., Reddy, J.N., Knight, N.F., 1992. Postbuckling response and failure prediction of graphite–epoxy plates loaded in compression. AIAA Journal 30, 2106–2113.

Jensen, D.W., Lagace, P.A., 1988. Influence of mechanical couplings on the buckling and postbuckling of anisotropic plates. AIAA Journal 26, 1269–1277.

Kardomateas, G.A., Simitses, G.J., Shen, L., Li, R., 2002. Buckling of sandwich wide columns. International Journal of Non-Linear Mechanics 37, 1239–1247.

Leissa, A.W., 1987. A review of laminated composite plate buckling. Applied Mechanics Reviews 40, 575–591.

Librescu, L., Hause, T., 2000. Recent developments in the modeling and behavior of advanced sandwich constructions. Composite Structures 48, 1–17.

Librescu, L., Nemeth, M.P., Starnes, J.H., Lin, W., 2000. Nonlinear response of flat and curved panels subject to thermomechanical loads. Journal of Thermal Stresses 23, 549–582.

Meressi, S., Paden, B., 1993. Buckling control of a flexible beam using piezoelectric actuators. Journal of Guidance and Dynamics 26, 977–980.

Oh, I.K., Han, J.H., Lee, I., 2001. Thermopiezoelastic snapping of piezolaminated plates using nonlinear finite elements. AIAA Journal 39, 1188–1198.

Pai, P.F., Nayfeh, A.H., Oh, K., Mook, D.T., 1993. A refined nonlinear model of composite plates with integrated piezoelectric actuators and sensors. International Journal of Solids and Structures 30, 1603–1630.

Saravanos, D.A., 1997. Coupled mixed-field laminate theory and finite element for smart piezoelectric composite shell structures. AIAA Journal 35, 1327–1333.

Saravanos, D.A., Heyliger, P.R., 1999. Mechanics and computational models for laminated piezoelectric beams, plates and shells. Applied Mechanics Reviews 52, 305–320.

Starnes Jr., J.H., Rouse, M., 1981. Postbuckling and Failure Characteristics of Selected Flat Rectangular Graphite–Epoxy Plates Loaded in Compression. AIAA Paper 81-0543.

Tabiei, A., Simitses, G.J., 1997. Torsional instability of moderately thick composite cylindrical shells by various shells theories. AIAA Journal 35, 1243–1246.

Thomson, S.P., Loughlan, J., 1995. The active buckling control of some composite column using piezoceramic actuators. Composite Structures 32, 59–67.

Tzou, H.S., Bao, Y., 1997. Nonlinear piezothermoelasticity and multi-field actuations, Part 1: Nonlinear anisotropic piezothermoelastic shell laminates. Journal of Vibration and Acoustics 119, 374–381.

Tzou, H.S., Zhou, Y.H., 1997. Nonlinear piezothermoelasticity and multi-field actuations, Part 2: Control of nonlinear deflection, buckling and dynamics. Journal of Vibration and Acoustics. 119, 382–389.

Varelis, D., Saravanos, D.A., 2002a. Nonlinear coupled mechanics and initial buckling of composite plates with piezoelectric actuators and sensors. Journal of Smart Materials and Structures 11, 330–336.

Varelis, D., Saravanos, D.A., 2002b. Coupled Finite Element for The Non-linear Response of Laminated Piezoelectric Composite Structures. AIAA paper 2002-1442, 0th AIAA/ASME/AHS Adaptive Structures Conference, Denver, Colorado, April 22–25, 2002; AIAA Journal.